JHEP04(2008)045

Bicycling black rings

Henriette Elvang

Center for Theoretical Physics, Massachusetts Institute of Technology,
Cambridge, MA 02139, U.S.A.
E-mail: `elvang@lns.mit.edu`

Maria J. Rodriguez

Departament de Física Fonamental, Universitat de Barcelona,
Diagonal 647, E-08028, Barcelona, Spain, and
Department of Physics, University of California,
Santa Barbara, CA 93106, U.S.A.
E-mail: `majo@ffn.ub.es`

ABSTRACT: We present detailed physics analyses of two different 4+1-dimensional asymptotically flat vacuum black hole solutions with spin in two independent planes: the doubly spinning black ring and the bicycling black ring system ("bi-rings"). The latter is a new solution describing two concentric orthogonal rotating black rings which we construct using the inverse scattering technique. We focus particularly on extremal zero-temperature limits of the solutions. We construct the phase diagram of currently known zero-temperature vacuum black hole solutions with a single event horizon, and discuss the non-uniqueness introduced by more exotic black hole configurations such as bi-rings and multi-ring saturns.

Contents

1. Introduction

Black holes with zero temperature are of considerable interest since one has a good chance of understanding the microscopic origin of their physical properties, such as their entropy. Asymptotically flat supersymmetric black holes fall in this class of solutions, and there has been considerable progress in understanding their properties in string theory since the pioneering work of Strominger and Vafa [1]. Non-supersymmetric extremal black holes with

zero temperature are likewise of interest. Recent progress on understanding the microscopic nature of non-supersymmetric zero temperature black holes includes [2–8].

Non-supersymmetric black hole solutions are in general more difficult to work with, not just in terms of understanding their microscopics, but also because they are typically not easy to come by: exact solutions for non-supersymmetric black holes tend to be harder to construct than their supersymmetric cousins. This is in particular true for multi-centered solutions. With their harmonic functions, supersymmetric black holes can easily be superimposed, but non-supersymmetric systems can exhibit strong interactions between the individual black hole components, and the solutions are consequently more involved.

Application of integrability methods in higher-dimensional gravity has recently allowed progress on construction of new exact black hole vacuum solutions. For instance, the inverse scattering technique was used in the construction of the first asymptotically flat multi-black hole vacuum solution [9]. The solution — named "black saturn" for its characteristic appearance, a black ring balanced by rotation around a spherical black hole — exhibited clear signs of interactions, including gravitational frame-dragging. Other novel properties included a large degree of continuous non-uniqueness even for zero total angular momentum [9, 10]. The black saturn system, as constructed in [9], did not have a zero temperature limit. However, based on the results found in this paper, we propose the existence of an extremal zero-temperature black saturn solution, and we discuss the consequences of its expected continuous non-uniqueness for the phase diagram of extremal zero-temperature vacuum black holes.

In this paper we study two different 4+1-dimensional black hole systems with spin in the two independent planes of rotation, and we pay attention particularly to limits that give extremal zero temperature black hole configurations.

The first of these systems is a new vacuum solution which we call "bicycling black rings", or simply "bi-rings" for short. It is a balanced configuration of two singly spinning concentric black rings placed in orthogonal planes. Singly spinning means that they each carry "intrinsic" angular momentum only in the plane of the ring, i.e. spin along the S^1 direction of the horizon. One can think of the system as the superposition of two of the original black rings of [11] in orthogonal planes. This is sketched in figure 1. Note that the bi-ring solution is different from the so-called "di-ring" solutions [12, 13] where the two concentric rings lie in the same plane.

The bi-ring solution has three commuting Killing vectors ("U(1)^3 symmetry"): it is stationary, and the isometry of the S^1 of one ring is the isometry of the azimuthal angle of the S^2 of the other ring, and vice versa. We construct the solution using the inverse scattering method. The bi-ring solution exhibits 1-fold continuous non-uniqueness after balance conditions have been imposed. This freedom corresponds to distributing the total mass between the two black rings.

The two black rings in the bi-ring system interact with each other. The rotation of the S^1 of one ring affects the S^2 of the other by gravitational frame-dragging. This causes the S^2 to rotate, so each ring has two non-vanishing angular velocities corresponding to rotation in the two independent planes. The angular momentum of the S^2 is effectively bounded by the 3+1-dimensional Kerr bound. The solution has a zero temperature limit,
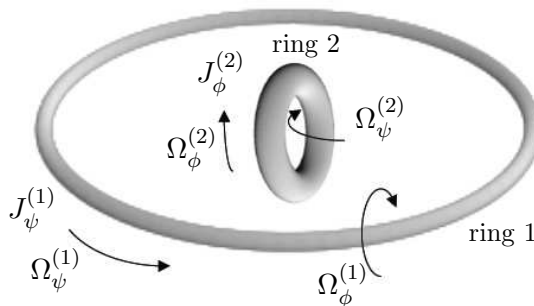
Figure 1: Bicycling black rings in orthogonal planes.

and in order to understand what happens in this limit we study in detail another solution, namely the doubly spinning black ring.

The doubly spinning black ring solution had long been anticipated. It is a single black ring balanced by angular momentum in the plane of the ring, but with angular momentum also in the orthogonal plane, corresponding to rotation of the two-sphere. Kudoh [17] found branches of this solution numerically, but the true breakthrough[1] was Pomeransky and Sen'kov's construction of the exact doubly spinning black ring solution [18]. They used a clever implementation of the inverse scattering method, and moreover presented the solution in the more intuitive ring-type coordinates [19] rather than axisymmetric coordinates which are natural for the solution generating technique. A more general unbalanced doubly spinning black ring solution has also been found [20].

We provide in this paper a detailed analysis of the physical properties of the Pomeransky-Sen'kov doubly spinning black ring [18]. These results have not previously been presented in the literature. Our results include the structure of the phases of doubly spinning black rings. We examine two different extremal zero-temperature limits. One is shown to result in a regular extremely spinning zero temperature black ring solution. The other limit appears to be singular, but this is just a coordinate singularity. A coordinate transformation shows that the resulting solution is nothing but the extremal doubly spinning Myers-Perry black hole, which is a regular black hole with zero temperature.

The zero-temperature limit of the bicycling black ring system is similar to the second extremal limit of the doubly spinning black ring, and thus we find evidence that the rings in this limit collapse to the extremal Myers-Perry black hole.

Inspired by the analysis of the bi-ring system and the doubly spinning black ring, we speculate about the structure of the phase diagram for zero-temperature black holes. It should be emphasized that our bi-ring solution is not the most general one. The obvious generalization is constructed from two doubly spinning black rings in orthogonal planes. In our discussion of the general phase diagram we consider the possibilities of generalized bicycling black rings as well as their even more exotic generalizations, which include multi-

---

[1]The unbalanced solution describing a black ring with rotation on the S^2 had been constructed by the inverse scattering method [14, 15], and also independently, in a simpler form, in [16].

bicycles (tandems) and bi-ring saturns. The richness of the phase structure of higher-dimensional black holes is striking, even in a limit as specialized as that of zero-temperature.

Supersymmetric versions of saturns, di-rings, bi-rings and many-ring systems can be constructed via superposition of the harmonic functions that characterize the individual black hole components of the system. This was first done for rings in [21]. Supersymmetric saturns with the black hole moved off the plane of the ring were studied in [22]. A key point in our analysis of the non-supersymmetric multi-black hole solutions is to track the interaction between the black holes in the system; this is not possible in the supersymmetric configurations where the mutual BPS-ness cancels out interaction effects.

The organization of the paper is as follows. We construct and analyze the bi-ring solution in section 2. In section 3 we study in detail a subfamily of the solutions where the two orthogonal rings are identical. We compare the results with a simple model obtained by superimposing two singly-spinning black rings and neglecting interactions. The doubly spinning black ring of [18] is analyzed in detail, and its physics discussed, in section 4. We describe in section 5 the zero temperature scaling limit of the bi-ring solution and argue that it corresponds to a collapse to a single extremal Myers-Perry black hole. We conclude with a discussion of zero temperature phases of 4+1-dimensional black holes in section 6. Two appendices are included: appendix A contains details of the horizon metric for the bi-ring solution, and appendix B reviews relevant properties of the Myers-Perry black hole [23].

Note: while this work was in progress, the paper [24] appeared, presenting also an orthogonal two-ring solution.

2. Bicycling black rings: construction and analysis

2.1 Construction

The inverse scattering method was recently used to construct the black saturn solution [9]. Our approach here is very similar, so we keep the presentation brief. The construction takes as input a seed solution on which we perform a series of "soliton transformations" and rescalings [25]. The transformations introduce new parameters, called Belinsky-Zakharov (BZ) parameters, which are organized in "BZ vectors". For definitions and review of the method, see [9]. We also refer the reader to [26 – 28] for literature on the inverse scattering technique and to [29] and [30] for Weyl solution techniques and rod diagram representations.

2.1.1 Seed solution

The seed solution is represented by the rod diagram given in figure 2. There are two negative density rods: one $[a_1, a_2]$ in the ψ-direction and the other $[a_6, a_7]$ in the ϕ-direction. These are included to facilitate adding angular momentum to each of the two black rings [9].

The corresponding seed metric is given by

$$ds^2 = (G_0)_{ab} \, dx^a dx^b + e^{2\nu_0} \left(d\rho^2 + dz^2 \right) \tag{2.1}$$
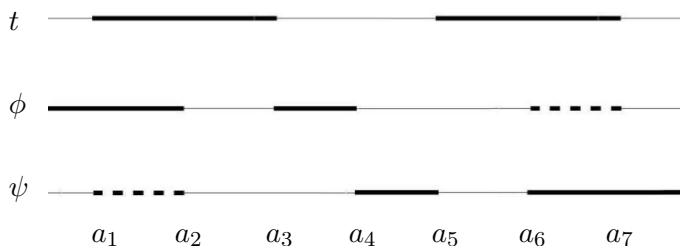
Figure 2: Rod configuration representing the sources for the seed metric G_0. Solid black lines in the figure correspond to rod sources of uniform density $+1/2$ and the dashed rods to uniform densities $-1/2$.

where $x^a = (t, \phi, \psi)$ and[2]

$$G_0 = \text{diag}\left\{ -\frac{\mu_1\,\mu_5}{\mu_3\,\mu_7},\ \frac{\rho^2\,\mu_3\,\mu_7}{\mu_2\,\mu_4\,\mu_6},\ \frac{\mu_2\,\mu_4\,\mu_6}{\mu_1\,\mu_5} \right\},\tag{2.2}$$

$$e^{2\nu_0} = \frac{\mu_2\mu_4\mu_6}{\mu_1\mu_5}\ \frac{\left(\prod_{1\leq i<j\leq 7} Z_{ij} \right)}{\left[Z_{15}Z_{26}Z_{37}Z_{24}Z_{46} \right]^3 \left(\prod_{i=1}^{7} Z_{ii} \right)}\ .\tag{2.3}$$

We use

$$\mu_i = \sqrt{\rho^2 + (z-a_i)^2} - (z-a_i)\,,\tag{2.4}$$

where the a_i are the rod endpoints, and we have introduced

$$Z_{ij} = \rho^2 + \mu_i\mu_j\,.\tag{2.5}$$

Note that $\det G_0 = -\rho^2$.

We assume the ordering

$$a_1 < a_2 < a_3 < a_4 < a_5 < a_6 < a_7\tag{2.6}$$

of the rod endpoints. When $a_6 = a_7$ and $a_4 = a_5$ the solution reduces to the seed solution used to construct black saturn. With its naked singularities (due to the negative density rods) the seed solution is not by itself of physical interest. As shown in [9], the soliton transformations which add angular momentum to the solution also make it possible to fully eliminate the naked singularities.

2.1.2 The 2-soliton transformation

We construct the bicycling black ring solution as follows (see [9] for details):

1. Perform the following two 1-soliton transformations on the seed solution (2.2):

   - Remove an anti-soliton at $z = a_1$ with trivial BZ vector (1,0,0); this is equivalent to dividing $(G_0)_{tt}$ by $-\rho^2/\bar{\mu}_1^2 = -\mu_1^2/\rho^2$.

---

[2]An integration constant in $e^{2\nu_0}$ is set to one in order to make the final solution asymptotically flat.

- Remove a soliton at $z = a_7$ with trivial BZ vector (1,0,0); this is equivalent to dividing $(G_0)_{tt}$ by $\left(-\rho^2/\mu_7^2\right)$.

The result is the metric matrix

$$G_0' = \text{diag}\left\{ -\frac{\mu_5\,\mu_7}{\mu_1\,\mu_3},\ \frac{\rho^2\,\mu_3\,\mu_7}{\mu_2\,\mu_4\,\mu_6},\ \frac{\mu_2\,\mu_4\,\mu_6}{\mu_1\,\mu_5} \right\}\,. \tag{2.7}$$

2. Rescale G_0' by a factor of $-\frac{\mu_1}{\mu_7}$ to find

$$\tilde{G}_0 = -\frac{\mu_1}{\mu_7}G_0' = \text{diag}\left\{ \frac{\mu_5}{\mu_3},\ \frac{\mu_1\,\bar{\mu}_2\,\mu_3}{\mu_4\,\mu_6},\ -\frac{\mu_2\,\mu_4\,\mu_6}{\mu_5\,\mu_7} \right\}\,, \tag{2.8}$$

where $\bar{\mu}_2 = -\rho^2/\mu_2$. This will be the seed for the next soliton transformation.

3. The generating matrix can be found from $\tilde{G}_0$. It is

$$\tilde{\Psi}_0(\lambda, \rho, z) = \text{diag}\left\{ \frac{(\mu_5-\lambda)}{(\mu_3-\lambda)},\ \frac{(\mu_1-\lambda)(\bar{\mu}_2-\lambda)(\mu_3-\lambda)}{(\mu_4-\lambda)(\mu_6-\lambda)},\ -\frac{(\mu_2-\lambda)(\mu_4-\lambda)(\mu_6-\lambda)}{(\mu_5-\lambda)(\mu_7-\lambda)} \right\}. \tag{2.9}$$

Note $\tilde{\Psi}(0, \rho, z) = \tilde{G}_0$.

4. Perform now a 2-soliton transformation with $\tilde{G}_0$ as seed:

- Add an anti-soliton at $z = a_1$ (pole at $\lambda = \bar{\mu}_1$) with BZ vector $m_0^{(1)} = (1, 0, c_1)$, and
- Add a soliton at $z = a_7$ (pole at $\lambda = \mu_7$) with BZ vector $m_0^{(2)} = (1, b_2, 0)$.

Denote the resulting metric $\tilde{G}$. The constants c_1 and b_2 are the BZ parameters of the transformation.

5. Rescale $\tilde{G}$ to find

$$G = -\frac{\mu_7}{\mu_1}\tilde{G}\,. \tag{2.10}$$

This is needed to undo the rescaling of step 2, so that $\det G = -\rho^2$.

6. The metric factor $e^{2\nu}$ is constructed using eq. (2.14) of [9].

The result $(G, e^{2\nu})$ is the final solution.

2.1.3 Solution

The bicycling black ring solution can be written as

$$ds^2 = -\frac{H_y}{H_x}\left[dt - \frac{\omega_\phi}{H_y}d\phi - \frac{\omega_\psi}{H_y}d\psi\right]^2 + H_y^{-1}\left[G_x d\phi^2 + G_y d\psi^2 - 2J_{xy}d\phi d\psi\right] + P H_x\left[d\rho^2 + dz^2\right].$$

We have written $e^{2\nu} = P H_x$. The metric is given in terms of the functions:

$$P = \frac{\mu_2\, Z_{23}\, Z_{25}\, Z_{34}\, Z_{35}\, Z_{36}\, Z_{45}\, Z_{47}\, Z_{56}\, Z_{57}\, Z_{67}}{\mu_1\, \mu_5^4\, \mu_7\, (\mu_3-\mu_7)^4\, Z_{12}\, Z_{13}\, Z_{14}\, Z_{15}^2\, Z_{16}\, Z_{17}\, Z_{24}^2\, Z_{26}^2\, Z_{27}\, Z_{37}^2\, Z_{46}^2\left[\prod_{i=1}^7 Z_{ii}\right]}\,, \tag{2.11}$$

(the Z_{ij} are defined in (2.5)),

$$H_x = \left(M_0 + c_1^2 \, M_1 + b_2^2 \, M_2 - c_1^2 \, b_2^2 \, M_3 \right), \tag{2.12}$$

$$H_y = \frac{\mu_5}{\mu_3} \left(\frac{\mu_1}{\mu_7} M_0 - c_1^2 \, \frac{\rho^2}{\mu_1 \, \mu_7} M_1 - b_2^2 \, \frac{\mu_1 \, \mu_7}{\rho^2} M_2 - c_1^2 \, b_2^2 \, \frac{\mu_7}{\mu_1} M_3 \right), \tag{2.13}$$

$$G_x = \frac{\mu_1 \, \mu_5 \, \rho^2}{\mu_2 \, \mu_4 \, \mu_6} \left(M_0 - c_1^2 \, \frac{\rho^2}{\mu_1^2} M_1 + b_2^2 \, M_2 + c_1^2 \, b_2^2 \, \frac{\rho^2}{\mu_1^2} M_3 \right), \tag{2.14}$$

$$G_y = \frac{\mu_2 \, \mu_4 \, \mu_6}{\mu_3 \, \mu_7} \left(M_0 + c_1^2 \, M_1 - b_2^2 \, \frac{\mu_7^2}{\rho^2} M_2 + c_1^2 \, b_2^2 \, \frac{\mu_7^2}{\rho^2} M_3 \right), \tag{2.15}$$

and

$$\begin{aligned} J_{xy} &= c_1 \, b_2 \, \rho^2 \, \mu_1 \mu_2 \, \mu_3 \, \mu_4 \, \mu_5^2 \, \mu_6 \, (\mu_3 - \mu_7)^2 (\mu_4 - \mu_7)(\mu_5 - \mu_7)(\mu_6 - \mu_7) \\ &\quad \times Z_{11} \, Z_{77} \, Z_{12} \, Z_{13} \, Z_{14} \, Z_{15}^2 \, Z_{16} \, Z_{17} \, Z_{27} \,, \end{aligned} \tag{2.16}$$

with

$$M_0 = \mu_4 \, \mu_5^3 \, \mu_6 \, \mu_7 \, (\mu_3 - \mu_7)^4 \, Z_{12}^2 \, Z_{13}^2 \, Z_{14}^2 \, Z_{16}^2 \, Z_{17}^2 \, Z_{27}^2 \,, \tag{2.17}$$

$$M_1 = \rho^2 \, \mu_1^2 \, \mu_2 \, \mu_3 \, \mu_4^2 \, \mu_5 \, \mu_6^2 \, (\mu_1 - \mu_7)^2 \, (\mu_3 - \mu_7)^4 \, Z_{15}^4 \, Z_{17}^2 \, Z_{27}^2 \,, \tag{2.18}$$

$$M_2 = \rho^4 \, \mu_1 \, \mu_2 \, \mu_3^2 \, \mu_5^2 \, \mu_7 \, (\mu_4 - \mu_7)^2 \, (\mu_5 - \mu_7)^2 \, (\mu_6 - \mu_7)^2 \, Z_{12}^2 \, Z_{13}^2 \, Z_{14}^2 \, Z_{16}^2 \,, \tag{2.19}$$

$$M_3 = \rho^4 \, \mu_1^3 \, \mu_2^2 \, \mu_3^3 \, \mu_4 \, \mu_6 \, (\mu_4 - \mu_7)^2 \, (\mu_5 - \mu_7)^2 \, (\mu_6 - \mu_7)^2 \, Z_{15}^4 \, Z_{17}^2 \,. \tag{2.20}$$

Finally we also have

$$\omega_\psi = c_1 \, \frac{Z_{11}}{\mu_1} \sqrt{\frac{\mu_2 \, \mu_4 \, \mu_6}{\mu_3 \, \mu_7 \, \rho^2}} \left(\sqrt{M_0 \, M_1} + b_2^2 \, \frac{\mu_7}{\rho} \sqrt{M_2 \, M_3} \right), \tag{2.21}$$

$$\omega_\phi = b_2 \, \frac{Z_{77}}{\mu_7} \sqrt{\frac{\mu_1 \, \mu_5}{\mu_2 \, \mu_4 \, \mu_6}} \left(\sqrt{M_0 \, M_2} + c_1^2 \, \frac{\rho}{\mu_1} \sqrt{M_1 \, M_3} \right). \tag{2.22}$$

Note that changing the sign of the BZ parameter c_1, $c_1 \to -c_1$ is equivalent to reversing the direction of rotation by taking $\psi \to -\psi$. Likewise, $b_2 \to -b_2$ simply corresponds to taking $\phi \to -\phi$. Thus we choose c_1 and b_2 to be negative without loss of generality. This choice gives positive angular momenta and angular velocities.

2.2 Analysis

2.2.1 Parameterization

The solution is parameterized by the rod endpoints a_i and the two BZ parameters c_1 and b_2. The parameters are all dimensionful. It is convenient to introduce an overall scale L,

$$L^2 = a_7 - a_1 \,, \tag{2.23}$$

and then express the solution in terms of dimensionless parameters κ_i defined as

$$\kappa_i = \frac{a_{i+1} - a_1}{L^2} \tag{2.24}$$

for $i = 1, 2, \ldots, 5$. The ordering (2.6) implies that

$$0 \leq \kappa_1 \leq \kappa_2 \leq \kappa_3 \leq \kappa_4 \leq \kappa_5 \leq 1 \,. \tag{2.25}$$

It is also useful to shift the z coordinate as

$$z = L^2 \bar{z} + a_1 \,, \tag{2.26}$$

so that $\bar{z}$ is dimensionless.

An analysis of the metric components G_{ab}, $a, b = t, \psi, \phi$, near the rod endpoints shows that there are divergences near $\bar{z} = 0$ and $\bar{z} = 1$, i.e. near $z = a_1$ and $z = a_7$. Just as for the black saturn solution, these singularities can be eliminated by an appropriate choice of the BZ parameters. This fixes c_1 and b_2 to be[3]

$$c_1 = -\frac{L\sqrt{2\,\kappa_1\,\kappa_2\,\kappa_3\,\kappa_5}}{\kappa_4}\,, \qquad b_2 = -L(1-\kappa_2)\sqrt{\frac{2(1-\kappa_1)}{(1-\kappa_3)(1-\kappa_4)(1-\kappa_5)}}\,. \tag{2.27}$$

In what follows we will always impose the smoothness conditions (2.27). The $\rho = 0$ metric is then smooth across $\bar{z} = 0$ and $\bar{z} = 1$, and there are no signs of the negative density rods of the seed solution. We describe the rod configuration of the bicycling black ring solution in the next subsection.

With c_1 and b_2 fixed by (2.27), the full solution is parametrized by the five κ_i-parameters, subject to the ordering (2.25), and the scale L.

2.2.2 Rod structure

Imposing (2.27) the rod structure can be summarized as (see figure 3):

- The semi-infinite rod $]-\infty, \kappa_1]$ and the finite rod $[\kappa_2, \kappa_3]$ have direction $(0, 1, 0)$.

- The semi-infinite rod $[\kappa_5, \infty[$ and the finite rod $[\kappa_3, \kappa_4]$ have direction $(0, 0, 1)$.

- The finite rod $[\kappa_1, \kappa_2]$ corresponds to a black ring whose horizon has the S^1 parameterized by ψ and the S^2 by (z, ϕ). This rod has direction $(1, \Omega_\phi^{(1)}, \Omega_\psi^{(1)})$.

  Likewise, the finite rod $[\kappa_4, \kappa_5]$ corresponds to a black ring whose horizon has the S^1 parameterized by ϕ and the S^2 by (z, ψ). This rod has direction $(1, \Omega_\phi^{(2)}, \Omega_\psi^{(2)})$.

The angular velocities are

$$\Omega_\phi^{(1)} = \frac{1}{L(1-\kappa_2)}\sqrt{\frac{(1-\kappa_3)(1-\kappa_4)(1-\kappa_5)}{2(1-\kappa_1)}}\,, \qquad \Omega_\psi^{(1)} = \frac{\kappa_4}{L}\sqrt{\frac{\kappa_1}{2\,\kappa_2\,\kappa_3\,\kappa_5}}\,, \tag{2.28}$$

$$\Omega_\phi^{(2)} = \frac{1-\kappa_2}{L}\sqrt{\frac{(1-\kappa_5)}{2(1-\kappa_1)(1-\kappa_3)(1-\kappa_4)}}\,, \qquad \Omega_\psi^{(2)} = \frac{1}{L\,\kappa_4}\sqrt{\frac{\kappa_1\,\kappa_2\,\kappa_3}{2\,\kappa_5}}\,. \tag{2.29}$$

We use superscripts (i), $i = 1, 2$, for the quantities associated with ring 1 (horizon located at $\rho = 0$ and $\kappa_1 \leq z \leq \kappa_2$) and ring 2 (horizon at $\rho = 0$ and $\kappa_4 \leq z \leq \kappa_5$).

---

[3]Changing the sign of the BZ parameters corresponds to reversing the sense of rotating of the rings, so without loss of generality we have assumed c_1 and b_2 to be negative.
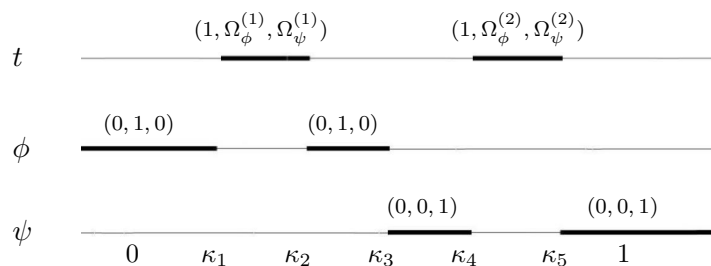
Figure 3: Rod structure of the regular bicycling black ring solution. Rod directions are shown over each rod.

Exchange symmetry. The rod picture figure 3 suggests that the solution has a symmetry corresponding to interchanging the two black rings. Indeed we have confirmed that the transformation

$$\kappa_1 \to 1 - \kappa_5\,, \qquad \kappa_2 \to 1 - \kappa_4\,, \qquad \kappa_3 \to 1 - \kappa_3\,, \qquad \kappa_4 \to 1 - \kappa_2\,, \qquad \kappa_5 \to 1 - \kappa_1\,,$$
$$\bar{z} \to 1 - \bar{z}\,, \qquad \psi \leftrightarrow \phi\,,$$

exchanges the physical parameters of the two black rings, as well as their balance conditions.[4]

2.2.3 Asymptotics and balance

The solution (2.11) is asymptotically flat. To see this, introduce asymptotic coordinates (r, θ) as $\rho = \frac{1}{2} r^2 \sin 2\theta$ and $z = \frac{1}{2} r^2 \cos 2\theta$. In the asymptotic limit $r \to \infty$, the metric then approaches

$$ds^2 = -dt^2 + dr^2 + r^2(d\theta^2 + \sin^2 \theta \, d\psi^2 + \cos^2 \theta \, d\phi^2)\,. \tag{2.30}$$

Regularity conditions[5] require the angular coordinates ϕ and ψ have periods 2π,

$$\Delta\phi = 2\pi\,, \qquad \Delta\psi = 2\pi\,, \tag{2.31}$$

so indeed the metric is asymptotically flat.

Regularity on the rods $[\kappa_2, \kappa_3]$ and $[\kappa_3, \kappa_4]$ requires non-trivial conditions,

$$1 = \frac{\Delta\phi}{2\pi} = \frac{\sqrt{\kappa_3\kappa_5(1 - \kappa_1)(\kappa_3 - \kappa_2)(\kappa_4 - \kappa_1)(\kappa_4 - \kappa_2)(\kappa_5 - \kappa_2)}}{\kappa_4(1 - \kappa_2)(\kappa_3 - \kappa_1)(\kappa_5 - \kappa_1)}\,, \tag{2.32}$$

$$1 = \frac{\Delta\psi}{2\pi} = \frac{\sqrt{\kappa_5(1 - \kappa_1)(1 - \kappa_3)(\kappa_4 - \kappa_1)(\kappa_4 - \kappa_3)(\kappa_4 - \kappa_2)(\kappa_5 - \kappa_2)}}{\kappa_4(1 - \kappa_2)(\kappa_5 - \kappa_1)(\kappa_5 - \kappa_3)}\,. \tag{2.33}$$

These are the conditions for balancing each of the two black rings. If not imposed, then there are disks of conical singularities inside the rings. When studying the physical properties of the bicycling ring system, we always impose both balance conditions.

---

[4]This is only true when the conditions (2.27) are imposed; if not imposed, one must in addition transform c_1 and b_2.

[5]The periodicities (2.31) follow from regularity conditions on the rods $]-\infty, \kappa_1]$ and $[\kappa_5, \infty[$. The general regularity condition is that when $G_{\phi\phi} \to 0$ as $\rho \to 0$ then $\Delta\phi = 2\pi \lim_{\rho \to 0} \sqrt{\frac{\rho^2 G_{\rho\rho}}{G_{\phi\phi}}}$. Likewise for ψ.

Solving the balance conditions. We briefly outline the strategy for solving the balance conditions in practical applications. This is used in section 5. The squared ratio of (2.32) and (2.33) is

$$1 = \frac{\kappa_3 \, (\kappa_3 - \kappa_2)(\kappa_5 - \kappa_3)^2}{(1 - \kappa_3)(\kappa_4 - \kappa_3)(\kappa_3 - \kappa_1)^2} \,. \tag{2.34}$$

This condition is linear in κ_2 and κ_4; solving for κ_4 gives

$$\kappa_4 = \kappa_4^* \equiv \kappa_3 + \frac{\kappa_3(\kappa_3 - \kappa_2)(\kappa_5 - \kappa_3)^2}{(1 - \kappa_3)(\kappa_3 - \kappa_1)^2} \,. \tag{2.35}$$

Clearly $\kappa_3 \leq \kappa_4^*$, but we must also require that $\kappa_4^* \leq \kappa_5$, and that restricts the parameters on the r.h.s. of (2.35). The simplest way to express this is as an upper bound on κ_5,

$$\kappa_5 \leq \kappa_{5\mathrm{MAX}}(\kappa_1, \kappa_2, \kappa_3) \equiv \frac{\kappa_1^2 \, (1 - \kappa_3) - 2 \, \kappa_1 \, \kappa_3 \, (1 - \kappa_3) + \kappa_3^2 \, (1 - \kappa_2)}{\kappa_3 \, (\kappa_3 - \kappa_2)} \,. \tag{2.36}$$

This condition ensures $\kappa_3 \leq \kappa_4^* \leq \kappa_5$.

Plugging (2.35) into either of the balance conditions (2.32) or (2.33) we obtain a polynomial equation which is 8th order in κ_1, 4th order in κ_2, 7th order in κ_3, and 6th order in κ_5. Solving this condition for κ_2 seems to be the simplest. As a fourth order polynomial, one can obtain the roots analytically, but in applications we will simply solve numerically for κ_2 in order to impose balance. For given κ_1, κ_3, and κ_5, we select the real root(s) κ_2^* which satisfy (a) $\kappa_1 < \kappa_2^* < \kappa_3$, and (b) $\kappa_5 \leq \kappa_{5\mathrm{MAX}}(\kappa_1, \kappa_2^*, \kappa_3)$.

Imposing both balance conditions leaves the bi-ring solution with three dimensionless parameters $0 < \kappa_1 < \kappa_3 < \kappa_5 < 1$ and the scale L. Fixing the total ADM mass fixes the scale. Fixing further the only other conserved quantities, namely the two angular momenta, leaves a single free parameter. This continuous non-uniqueness parameter corresponds to the freedom of distributing the total mass between the two black rings.

2.2.4 Physical parameters

The ADM mass and angular momenta are

$$M = \frac{3\pi \, L^2}{4G_5}(1 + \kappa_2 - \kappa_4) \,, \tag{2.37}$$

$$J_\psi = \frac{\pi \, L^3}{\sqrt{2} \, G_5} \frac{\sqrt{\kappa_1 \, \kappa_2 \, \kappa_3 \, \kappa_5}}{\kappa_4} \,, \tag{2.38}$$

$$J_\phi = \frac{\pi \, L^3}{\sqrt{2} \, G_5} \frac{\sqrt{(1 - \kappa_1)(1 - \kappa_3)(1 - \kappa_4)(1 - \kappa_5)}}{(1 - \kappa_2)} \,. \tag{2.39}$$

The mass is always positive.

We analyze the black ring horizons in appendix A. The horizon area and temperature of each black ring are found to be

$$A_{\mathrm{H}}^{(1)} = (2\pi)^2 \, L^3 \, (\kappa_2 - \kappa_1) \frac{\sqrt{2 \, \kappa_2 \, \kappa_3 \, \kappa_5 \, (1 - \kappa_1)(\kappa_2 - \kappa_1)(\kappa_4 - \kappa_1)}}{\kappa_4 \, (\kappa_3 - \kappa_1)(\kappa_5 - \kappa_1)} \,, \tag{2.40}$$

$$A_{\mathrm{H}}^{(2)} = (2\pi)^2 \, L^3 \, (\kappa_5 - \kappa_4) \frac{\sqrt{2 \, \kappa_5 \, (1 - \kappa_1)(1 - \kappa_3)(1 - \kappa_4)(\kappa_5 - \kappa_4)(\kappa_5 - \kappa_2)}}{(1 - \kappa_2)(\kappa_5 - \kappa_1)(\kappa_5 - \kappa_3)} \,, \tag{2.41}$$

and

$$T_{\mathrm{H}}^{(1)} = \frac{\kappa_4 \, (\kappa_3 - \kappa_1)(\kappa_5 - \kappa_1)}{2\pi L \sqrt{2 \, \kappa_2 \, \kappa_3 \, \kappa_5 \, (1 - \kappa_1)(\kappa_2 - \kappa_1)(\kappa_4 - \kappa_1)}} \,, \tag{2.42}$$

$$T_{\mathrm{H}}^{(2)} = \frac{(1 - \kappa_2)(\kappa_5 - \kappa_1)(\kappa_5 - \kappa_3)}{2\pi L \sqrt{2 \, \kappa_5 \, (1 - \kappa_1)(1 - \kappa_3)(1 - \kappa_4)(\kappa_5 - \kappa_2)(\kappa_5 - \kappa_4)}} \,. \tag{2.43}$$

Smarr relations.   The bicycling rings satisfy the Smarr relation

$$\frac{2}{3}M = T_1 S_1 + T_2 S_2 + \Omega_\psi^{(1)} \, J_\psi + \Omega_\phi^{(2)} \, J_\phi \,, \tag{2.44}$$

where $S^{(i)} = A_{\mathrm{H}}^{(i)}/(4G)$. This holds independently of the balance conditions.

Komar integrals for the masses and angular momenta give

$$M^{(1)} = \frac{3\pi L^2}{4G} \, \kappa_2 \,, \qquad M^{(2)} = \frac{3\pi L^2}{4G} \, (1 - \kappa_4) \,. \tag{2.45}$$

and

$$J_\psi^{(1)} = J_\psi \,, \qquad J_\phi^{(1)} = 0 \,, \qquad J_\phi^{(2)} = J_\phi \,, \qquad J_\psi^{(2)} = 0 \,. \tag{2.46}$$

The Komar masses and angular momenta add up to the total ADM mass and ADM angular momenta, and they satisfy $M^{(i)} = \frac{3}{2}\big(T_{\mathrm{H}}^{(i)} S^{(i)} + \Omega_\psi^{(i)} \, J_\psi^{(i)}\big)$. This holds independently of the balance conditions, and should merely be viewed as a calculational check (see [10]) of our results for the physical parameters.

2.2.5 CTCs

It can analytically be shown that there are no closed timelike curves (CTCs) in the plane inside each rings. Outside the ring, in the plane of the ring, we have checked numerically near the ring and found no CTCs. We have also performed numerical checks in the bulk (off the planes of the rings), and no CTCs where found. Our checks are not exhaustive, and further progress may require a better coordinate system. We do not expect the solution to have naked CTCs, in particular we note that typical signs of CTCs are absent here, for instance the horizon area remains positive and well-defined for all admissible parameters.

3. Symmetric bicycles

Our bi-ring solution is described by a single scale and five dimensionless parameters, subject to two balance conditions. Thus for fixed ADM mass, there are three independent parameters for the balanced system. Asymptotically, the total angular momenta in the two planes fix two of these parameters. Thus the balanced bi-rings have 1-fold continuous non-uniqueness. This freedom corresponds to continuously distributing the total mass between the two black rings.

A particularly simple subclass of bi-ring solutions is obtained by requiring that the two black rings are identical; i.e. that they have the same temperatures, the same areas, and the same S^1 and S^2 angular velocities. We study this class of solutions in this section.

Please note that in this paper we do not review properties of singly spinning black rings and their thin and fat ring branches in the phase diagram. This has by now been explained in much detail in several papers. We refer in particular to [31] and the review [19].
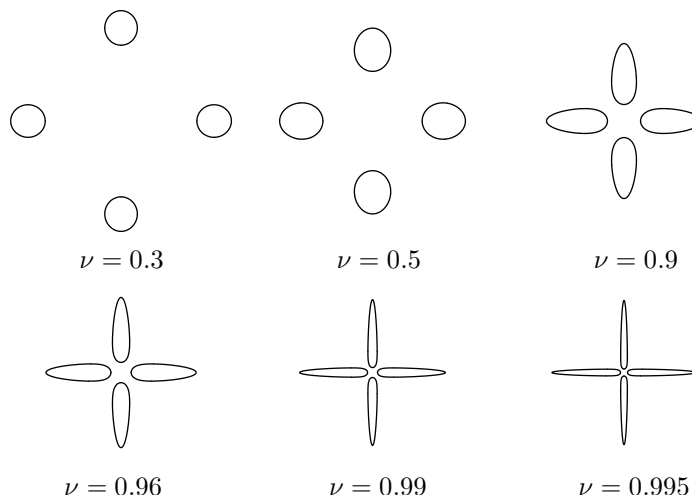
Figure 4: Visualization of the symmetric bicycling black ring system. Shown is the superposition of two identical singly spinning rings in orthogonal planes for six different values of the angular momentum $j_\psi = j_\phi = \sqrt{(1+\nu)^3/(8\nu)}$ (recall [10] that $0 < \nu < 1/2$ for the thin ring branch and $1/2 < \nu < 1$ on the fat black ring branch). The total mass is fixed to be the same for each plot. The embeddings are plotted on the same scale. Interactions between the two rings are ignored in this model, but in the real bi-ring solution interactions play an important role.

3.1 A model

Before examining in detail the symmetric bi-ring configuration, it is useful to first model the system by superimposing two singly spinning rings in orthogonal planes. This of course ignores the interactions between the two rings, the significance of which we soon discover. A similar model for black saturn was studied in [10].

The first purpose of the model is to illustrate the geometry of the 2-ring configuration. This is done for six different values of the angular momentum in figure 4. In each case we have plotted, for two identical copies of singly spinning black ring, the isometric embeddings of the diametrical cross section of the ring S^2's, separated by the inner horizon radius. These quantities, as well as further details on black ring geometry and isometric embeddings, can be found in [31].

Black rings on the thin ring branch have two-spheres which are nearly spherical and largely separated. As the angular momentum decreases so does the inner horizon radius, and the S^2 of the horizon deforms as shown in figure 4. For the singly spinning black ring, the inner radius can become arbitrarily small, and as it goes to zero the solution becomes nakedly singular. In the model the inner horizon radius can also take arbitrarily small values, but this of course ignores interactions between the two rings.

The second purpose of the 2-ring model is to examine what we may encounter in the

real bi-ring system. We introduce the usual fixed mass dimensionless variables

$$j^2 = \frac{27\,\pi}{32\,G}\frac{J^2}{M^3}\,, \qquad a_{\rm H} = \frac{3}{16}\sqrt{\frac{3}{\pi}}\frac{A_{\rm H}}{(G\,M)^{3/2}} \tag{3.1}$$

for angular momentum and horizon area. In order to balance itself against collapse, a singly spinning black ring must carry a certain amount of angular momentum for the given mass. This gives a lower bound on j, namely $27/32 \leq j^2$. At $j^2 = 27/32$, the ring has maximum horizon area, $a_{\rm H} = 1$. The singly spinning ring can rotate with arbitrarily high angular momentum, and as it does so the area goes to zero as $a_{\rm H} \sim (\sqrt{2}\,j)^{-1}$ for $j \to \infty$.

We normalize the physical parameters for the bi-rings in terms of the total mass. For the symmetric configuration, this is $2M$, with M the mass of each ring. The total area is $2A_{\rm H}$. In the limit where the rings are large and thin, they have little interaction and we expect the model to describe the system well. Using (3.1) with $2M$ as the total mass we find that for the symmetric bi-ring model, the total horizon area goes as $a_{\rm H}^{\rm total} \sim (4\sqrt{2}\,j)^{-1}$ for large j. This behavior is verified for the bi-ring solution in the next subsection.

Ignoring interactions we likewise estimate the bi-ring to have maximal area $a_{\rm H}^{\rm max} = 2/2^{3/2} = 1/\sqrt{2} \approx 0.7$ and minimum angular momentum $j_{\rm min}^2 = 1/2^3(27/32) \approx 0.11$. We show below that the actual values are $a_{\rm H}^{\rm max} \approx 0.485$ and $j_{\rm min}^2 \approx 0.246$ for the bi-ring solution. This indicates that interaction effects are important for black rings near the cusp where the rings in the bi-ring system are closer to each other.

A clear sign of interactions in the true bi-ring configuration is that the rotation of the S^1 of one ring drags the S^2 of the other ring into rotation. We study this in the next subsection.

3.2 The symmetric bi-ring phase

In the symmetric bi-ring configuration the two rings are identical: they have the same area and temperature, and the magnitudes of the angular momenta in the two planes of rotation are the same. It is easily verified that this is obtained from a symmetric rod configuration with

$$\kappa_5 = 1 - \kappa_1\,, \qquad \kappa_4 = 1 - \kappa_2\,, \qquad \kappa_3 = \frac{1}{2}\,. \tag{3.2}$$

The two balance conditions (2.32)-(2.33) are also identical, and an equilibrium configuration is is therefore obtained by imposing a single condition,

$$1 = \frac{(1-\kappa_1)(1-\kappa_1-\kappa_2)(1-2\kappa_2)}{(1-\kappa_2)^2(1-2\kappa_1)^2}\,. \tag{3.3}$$

The parameters must satisfy

$$0 < \kappa_1 < \kappa_2 < \frac{1}{2}\,, \tag{3.4}$$

and this selects one solution κ_2^* to the balance condition (3.3):

$$\kappa_2^* = \frac{1 + 3\kappa_1 - 6\kappa_1^2 - (1-2\kappa_1)\sqrt{1+2\kappa_1-3\kappa_1^2}}{2(1+2\kappa_1-4\kappa_1^2)}\,. \tag{3.5}$$
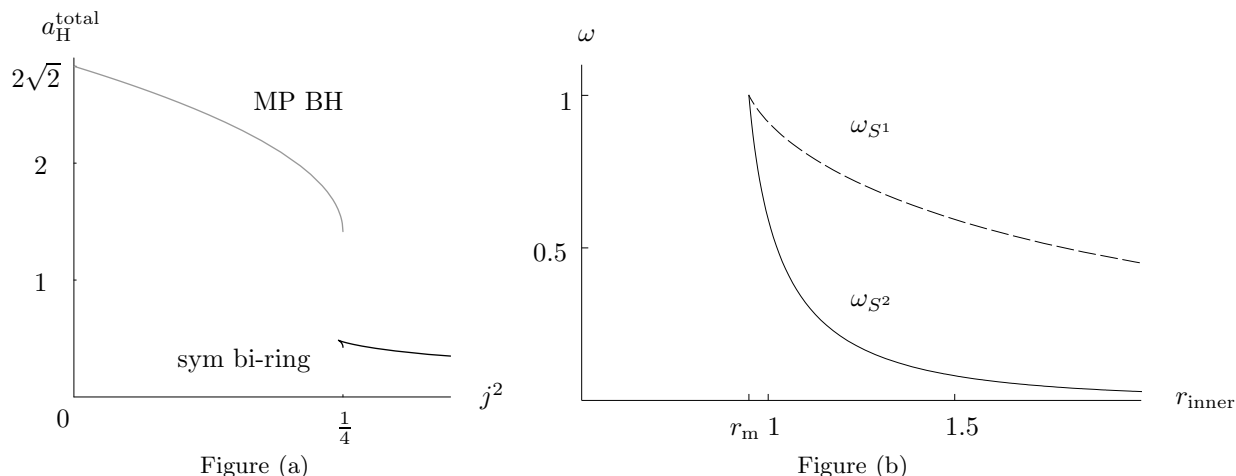
Figure 5: (a) Area a_H vs. j^2 for solutions with equal angular momenta in the two planes of rotation, $j \equiv j_\psi = j_\phi$. The *gray* curve shows the Myers-Perry black hole phase and the *black* curve is the symmetric bi-ring configuration. Both curves have endpoints at $j^2 = 1/4$. The solutions at the endpoints have finite area and zero temperature. (b) Angular velocities vs. inner horizon radius r_{inner}. The *solid* (*dashed*) curves corresponds to the angular velocity of the S^2 (S^1) of the horizon. The minimum inner radius is $r_m \approx 0.95$.

Thus the balanced symmetric bi-ring system is parameterized by a single parameter, κ_1. This is equivalent to a single balanced black ring which is parameterized by a single parameter.

Figure 5(a) shows the dimensionless area a_H vs. the angular momentum j^2 (as introduced in (3.1)) for the symmetric bi-ring system (black curve). As suggested by the model in the previous section, the angular momentum j of the symmetric bi-ring system is unbounded from above. When $\kappa_1 \to 0$, $j \to \infty$ and the area goes to zero as $a_H \sim (4\sqrt{2}\, j)^{-1}$, in exact agreement with the non-interacting model of the previous subsection. In this limit the model gives a good description of the system, since the rings are long and thin, hence far apart and with negligible interactions.

Just like the singly spinning black ring, there are two branches, a thin and a fat ring branch, and they meet at a cusp, where the area reaches its maximum and the angular momentum its minimum. At the cusp[6] the angular momentum and area take values $j^2_{\min} \approx 0.246$ and $a_{H\,\max} \approx 0.485$. The naive estimates of the non-interacting model in the previous subsection are different from the actual bi-ring results. We ascribe this to interactions between the two rings.

Each ring carries angular momentum in the plane of its S^1, and it does not have intrinsic angular momentum on the S^2 (the Komar angular momentum integral for the S^2 rotation vanishes). The 2-spheres are nonetheless rotating; they have non-vanishing angular velocity due to the interaction between the two rings. Through rotational frame-dragging, the S^1 rotation $J_\psi^{(1)}$ of ring 1 drags the S^2 of ring 2 to rotate with angular velocity $\Omega_\psi^{(2)}$. Ring 2 of course acts symmetrically on ring 1. Claiming that the effect is gravitational frame-dragging is of course an interpretation of the physical properties of the

---

[6]The cusp is located at $\kappa_1 = \frac{1}{6}\left(1 - 2^{4/3}\left(5 + \sqrt{57}\right)^{-1/3} + 2^{-1/3}\left(5 + \sqrt{57}\right)^{1/3}\right) \approx 0.293$.

solution, but it is very natural. The interpretation of similar dragging effects was tested in detail for the black saturn solution [9].

Figure 5(b) shows the S^1 angular velocity $\omega_\psi^{(1)}$ for ring 1 and the S^2 angular velocity $\omega_\psi^{(2)}$ for ring 2 plotted vs. the inner horizon radius r_{inner} of ring 1. (This is done for the symmetric bi-ring configuration, so there is really no distinction between parameters for ring 1 and ring 2.) The dimensionless angular velocity is defined as

$$\omega_i = \sqrt{\frac{8}{3\pi}}\, \Omega_i\, (G\,M)^{1/2}\,. \tag{3.6}$$

The inner horizon radius is the S^1 radius on the inside rim of the ring. Normalized by the total mass it is

$$r_{\text{inner}} = (GM)^{-1/2}\sqrt{G_{\psi\psi}}\,|_{\rho=0,\bar{z}=\kappa 2} = \sqrt{\frac{2(1-\kappa_1-\kappa_2)}{3\pi(\kappa_2-\kappa_1)}}\,. \tag{3.7}$$

The inner radius r_{inner} decreases monotonically along the symmetric ring branch in figure 5(a). As $j \to \infty$, $r_{\text{inner}} \to \infty$.

We use the inner horizon radius as a rough estimate of the spatial separation between the two black rings. As shown in figure 5(b) the S^1 angular velocity ω_{S^1} increases monototically as the ring shrinks. As r_{inner} decreases, the S^2 spins faster and faster, reaching a maximum at $j^2 = 1/4$, where $\omega_{S^2} = \omega_{S^1} = 1$. Oppositely, as the separation between the ring becomes large, $r_{\text{inner}} \to \infty$ ($j \to \infty$), one finds that $\omega_{S^2} \to 0$. We also note that $\omega_{S^2} < \omega_{S^1}$. These observations are consistent with the interpretation that the S^2 spin is due to gravitational frame-dragging.

In figure 5(a) we also display the only other currently known vacuum black hole solution in 4+1 dimensions with *equal* magnitude angular momenta in the two planes of rotation: the Myers-Perry black hole with $J_\psi = J_\phi$ (gray curve in figure 5(a)). A few relevant properties of the Myers-Perry black hole are reviewed in appendix B. At $j = 0$ this is just the 4+1-dimensional Schwarzschild black hole whose area is $a_{\text{H}} = 2\sqrt{2}$. As j increases, the area decreases, and the curve ends at finite area.[7] The endpoint solution is a maximally rotating extremal zero temperature black hole with $j^2 \equiv j_\phi^2 = j_\psi^2 = 1/4$ and $a_{\text{H}} = \sqrt{2}$.

The symmetric bi-ring branch in figure 5(a) also has an endpoint at $j^2 \equiv j_\phi^2 = j_\psi^2 = 1/4$, and indeed in this limit,[8] the temperature goes to zero. It is tempting to interpret the endpoint of the symmetric bi-ring branch as an extremal zero temperature bi-ring configuration. However, examining a similar limit of the doubly spinning black ring in the next section, we are instead lead to the conclusion that the $j^2 \to 1/4$ limit of the symmetric bi-ring corresponds to a collapse of the rings to the symmetric zero temperature Myers-Perry black

---

[7]Contrary to the singly spinning Myers-Perry black hole which ends at $j = 1$ and $a_{\text{H}} = 0$, where it is singular.

[8]The limit is $\kappa_1 \to 1/2$, corresponding to a collapse of *all* the finite length rods in the phase diagram. Due to the balance condition, this particular scaling limit results in a non-trivial solution. The extremal limits of the Kerr black hole and the 4+1d Myers-Perry black hole also correspond to a controlled collapses of the horizon rods. This seems to be a general feature of zero temperature black holes.

hole. In such a collapse, the horizon area will change discontinuously. Thus the $j^2 = 1/4$ endpoint of the symmetric bi-ring curve in figure 5(a) is not part of the bi-ring phase.

Naturally one expects the existence of more general bi-ring systems in which each ring carries intrinsic angular momentum in both planes of rotation. Such solutions will extend the class of symmetric bi-rings, and their phases must also be considered for the full structure of the phase diagram figure 5(a). Placing a black hole at the center of such a generalized bi-ring system will give rise to an even larger class of solutions, including symmetric ones. Further discussion of generalizations follows in section 6.

4. Doubly spinning black rings

The solution for the *balanced* doubly spinning black ring was presented by Pomeransky and Sen'kov [18]. We provide here an analysis of the doubly spinning ring solution and its physical properties.

4.1 Analysis

We use the solution[9] in the form presented in [18] except that we interchange ϕ and ψ, so that ϕ is the azimuthal angle of the S^2 and ψ parameterizes the circle of the ring.

The solution [18] is given in ring coordinates (x, y) with $|x| \leq 1$ and $y \leq -1$, and is parametrized by a scale k and two dimensionless parameters λ and ν which are required to satisfy

$$0 \leq \nu < 1, \qquad 2\sqrt{\nu} \leq \lambda < 1 + \nu. \tag{4.1}$$

The balanced black ring [11] with rotation only in the plane of the ring is found in the limit $\nu \to 0$. The unbalanced black ring with angular momentum only on the S^2 [14 – 16] cannot be obtained from the Pomeransky-Sen'kov solution because the balance condition is imposed in the solution presented in [18]. Likewise it is not possible to obtain the full general 5-dimensional Myers-Perry black hole as a "collapse" limit of the balanced ring solution. The more general unbalanced doubly spinning black ring metric of Morisawa et al [20] contains these limits.

Asymptotics. Asymptotic coordinates (ρ, θ) are introduced through the coordinate transformation

$$x = -1 + 4k^2 \alpha^2 \frac{1}{\rho} \cos^2 \theta, \qquad y = -1 - 4k^2 \alpha^2 \frac{1}{\rho} \sin^2 \theta, \qquad \alpha = \sqrt{\frac{1 + \nu - \lambda}{1 - \lambda}}. \tag{4.2}$$

In the $\rho \to \infty$ limit this brings the metric of [18] to a manifestly flat form with the angular coordinates ϕ, ψ and the time coordinate t canonically normalized.

---

[9]We have analytically verified that the solution presented in [18] indeed satisfies the Einstein vacuum equations, $R_{\mu\nu} = 0$.

Horizon. The roots of the equation

$$1 + \lambda\, y + \nu\, y^2 = 0 \tag{4.3}$$

determine the locations of the inner and outer horizons; the event horizon is located at

$$y_h = \frac{-\lambda + \sqrt{\lambda^2 - 4\nu}}{2\nu} \,. \tag{4.4}$$

The metric has a coordinate singularity at the roots of (4.3) where g_{yy} diverges. Good coordinates through the event horizon can be constructed by setting $\bar{y} = y - y_h$ and performing the coordinate transformation

$$d\bar{\phi} = d\phi - \frac{A}{\bar{y}}\, d\bar{y}\,, \qquad d\bar{\psi} = d\psi - \frac{B}{\bar{y}}\, d\bar{y}\,, \qquad d\bar{t} = dt - \frac{C}{\bar{y}}\, d\bar{y}\,. \tag{4.5}$$

The constants A, B, and C are determined by eliminating potential divergences in the metric components in the limit $\bar{y} \to 0$. In more detail: the constants A, C are fixed in terms of B (and λ, ν) by requiring the absence of a $1/\bar{y}$ divergence in $g_{t\bar{y}}$. This also eliminates similar potential divergences in $g_{\phi\bar{y}}$ and $g_{\psi\bar{y}}$. Next B can be chosen such that the divergences in $g_{\bar{y}\bar{y}}$ cancel. In the coordinates $(\bar{t}, \bar{\phi}, \bar{\psi}, x, \bar{y})$, the metric is then analytic across $\bar{y} = 0$, and $y = y_h$ is therefore the location of a regular event horizon. The analysis is valid for $2\nu^{1/2} < \lambda < 1 + \nu$.

An *extremal* rotating black ring is obtained for $\lambda = 2\sqrt{\nu}$, when the inner and outer horizons coincide (i.e. the roots of (4.3) coincide). Good coordinates through the horizon can also be found in this case, but it requires a separate analysis where terms $1/\bar{y}$ and $1/\bar{y}^2$ are both included in the coordinate transformations (4.5). It was shown in [32] that the near horizon geometry of the extremal black ring is isometric to the near horizon geometry of a special case of the boosted Kerr black string.

Physical parameters. The ADM mass and angular momenta are

$$M = \frac{3\pi\, k^2}{G} \frac{\lambda}{1 + \nu - \lambda}\,, \qquad J_\phi = \frac{4\pi\, k^3}{G} \frac{\lambda\, \sqrt{\nu\left[(1+\nu)^2 - \lambda^2\right]}}{(1 + \nu - \lambda)(1 - \nu)^2}\,, \tag{4.6}$$

$$J_\psi = \frac{2\pi\, k^3}{G} \frac{\lambda\,(1 + \lambda - 6\nu + \nu\,\lambda + \nu^2)\,\sqrt{(1+\nu)^2 - \lambda^2}}{(1 + \nu - \lambda)^2 (1 - \nu)^2}\,. \tag{4.7}$$

The angular velocities are

$$\Omega_\psi = \frac{1}{2k} \sqrt{\frac{1 + \nu - \lambda}{1 + \nu + \lambda}}\,, \qquad \Omega_\phi = \frac{\lambda(1+\nu) - (1-\nu)\sqrt{\lambda^2 - 4\nu}}{4k\,\lambda\sqrt{\nu}} \sqrt{\frac{1 + \nu - \lambda}{1 + \nu + \lambda}}\,, \tag{4.8}$$

and the horizon area can be written

$$A_{\mathrm{H}} = \frac{32\pi^2 k^3\, \lambda(1 + \nu + \lambda)}{(1 - \nu)^2 (y_h^{-1} - y_h)}\,. \tag{4.9}$$

The temperature can be found using the Smarr formula $\frac{2}{3}M = T_{\mathrm{H}}S + J_\phi\Omega_\phi + \Omega_\psi J_\psi$, with $S = A_{\mathrm{H}}/(4G)$, and the result is

$$T_{\mathrm{H}} = \frac{(y_h^{-1} - y_h)(1 - \nu)\sqrt{\lambda^2 - 4\nu}}{8\pi\, k\, \lambda(1 + \nu + \lambda)}\,. \tag{4.10}$$

– 17 –

As expected, $T_H = 0$ for the extremal solution with $\lambda = 2\sqrt{\nu}$.

Examining the ranges of the dimensionless angular momenta (defined in (3.1)) one finds

$$j_\phi \leq \frac{1}{4}, \qquad j_\psi \geq \frac{3}{4}, \tag{4.11}$$

In particular the angular momenta can never be equal, and the ratio j_ϕ/j_ψ is less than or equal to 1/3. The dimensionless angular velocities satisfy $0 < \omega_\psi \leq 1$ and $0 \leq \omega_\phi \leq 1$.

4.2 Phase diagram

We are interested in three main questions: (1) how the S^2 angular momentum J_ϕ changes the behavior of the spinning black ring, (2) which regions of the phase diagram is covered by the doubly spinning black rings, and (3) what are the zero temperature extremal limits. The answers are summarized in the phase diagrams in figure 6. There are several curves of interest in the phase diagram, and we shall discuss them in turn.

The extremal black ring limit $\boldsymbol{\lambda \to 2\nu^{1/2}}$. The extremal black ring with $\lambda = 2\nu^{1/2}$ is regular and has zero temperature. Physically it corresponds to the S^2 rotating maximally, i.e. saturating the Kerr bound. In this limit, the angular momentum j_ψ and the area a_H can be written directly as functions of j_ϕ:

$$j_\psi = \frac{1 + 8j_\phi^2}{8j_\phi}, \qquad a_H = 2\sqrt{2}\, j_\phi. \tag{4.12}$$

In figure 6 this extremal phase is shown as the solid black curve. It starts at $j_\psi = 3/4$, $j_\phi = 1/4$ and $a_H = 1/\sqrt{2}$, and the area decreases monotonically to zero as $j_\psi \to \infty$ ($j_\phi \to 0$). We conclude that there exists zero temperature black rings for any S^1 angular momentum $j_\psi > 3/4$.

In the extremal ring limit, $\lambda = 2\sqrt{\nu}$, the inner and outer horizon radii are the same $r^{(\text{inner})} = r^{(\text{out})}$. This is similar to the case of supersymmetric black rings [33–35, 21].

The second extremal limit $\boldsymbol{\nu \to 1, \lambda \to 2}$ is a collapse. A second extremal limit corresponds to the limit $\nu \to 1$. Due to the parameter restrictions (4.1), we have to take $\lambda \to 2$ as $\nu \to 1$. This must be done in a way that leaves dimensionless parameters finite, and that requires the ratio

$$\sigma = \frac{1 + \nu - \lambda}{(1 - \nu)^2} \tag{4.13}$$

to be finite in the limit. Solving this equation for λ and taking the limit $\nu \to 1^-$ gives

$$T_H = 0, \qquad j_\phi = \sigma, \qquad j_\psi = 1 - \sigma, \qquad a_H = \frac{4\sqrt{2}\,\sigma^{3/2}}{1 - \sqrt{1 - 4\sigma}}, \qquad \omega_{\psi,\phi} \to 1. \tag{4.14}$$

The (j_ψ^2, a_H) curve is shown in figure 6 (dashed curve). As we now show, this curve does *not* represent a phase of extremal rings.
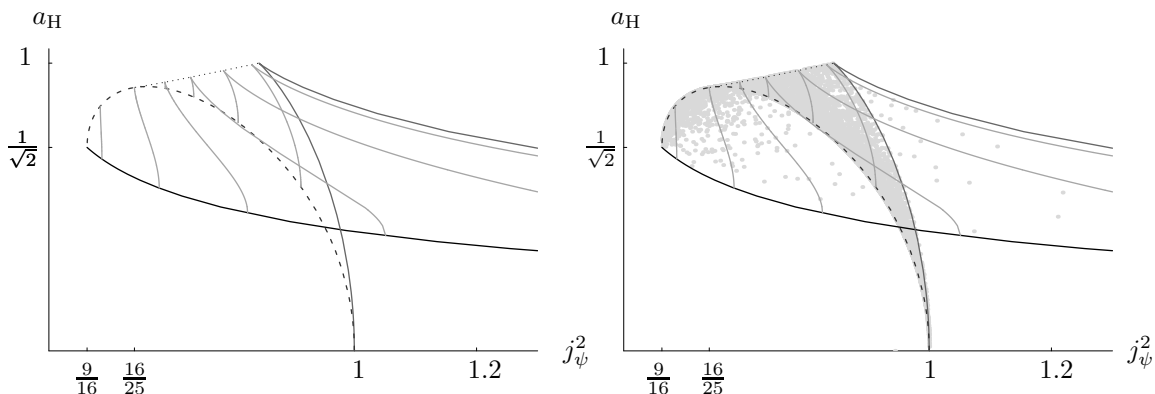
Figure 6: Phase diagrams for the doubly-spinning black ring: area vs. the S^1 angular momentum j_ψ^2. The *dark gray* curve shows the phase of the singly spinning black ring. The *light gray* curves are branches of constant j_ϕ; the particular values shown are (right towards left) $j_\phi^2 = \frac{1}{500}, \frac{1}{100}, \frac{1}{50}, \frac{1}{35}, \frac{1}{25}, \frac{1}{18}$. As $j_\phi^2 \to \frac{1}{16}$, its maximum value, the constant-j_ϕ curves degenerate to the point $j_\psi^2 = 9/16$ and $a_H = 1/\sqrt{2}$. Each of the light gray constant-j_ϕ curves start at the zero-temperature branch of doubly spinning black ring solutions, shown as the *solid black* curve, and they limit to the *black dashed* curve (see main text). The *black dotted* curve outlines the position of the cusp of the constant-j_ϕ curves; these are characterized by having minimum j_ψ and maximum area for given fixed j_ϕ. The plot on the right shows the same set of curves overlaying a scatter plot (*lighest gray* — 10,000 points) indicating the range in the phase diagram covered by doubly spinning black rings. The region is bounded by the curves we have described.

The limit $\nu \to 1, \lambda \to 2$ appears singular, but this is just a coordinate artifact, and the resulting solution is actually the extremal Myers-Perry black hole with parameters a_1, a_2 and $\mu^{1/2} = a_1 + a_2$. To see this, define

$$\mu = \frac{k^2}{(1-\nu)^2 \sigma}, \quad a_1 = \mu^{1/2}(1-\sigma), \quad a_2 = \mu^{1/2}\sigma, \tag{4.15}$$

and perform the following coordinate transformation

$$x = -1 + \frac{16\sqrt{a_2}\,k^3\cos^2\theta}{(a_1+a_2)^{3/2}(r^2-a_1a_2)}, \quad y = -1 - \frac{16\sqrt{a_2}\,k^3\sin^2\theta}{(a_1+a_2)^{3/2}(r^2-a_1a_2)}. \tag{4.16}$$

When $\nu \to 1$ one finds the metric for the extremal Myers-Perry solution. This limit is very similar to the Myers-Perry limit of singly spinning black rings, as presented for instance in appendix A of [3].

In this collapse limit of the ring to an extremal Myers-Perry black hole, the area is discontinuous, just like in the similar collapse limits of supersymmetric black rings [34]. So the dashed curve in figure 6 does not itself represent a phase of black rings, but it marks the endpoint of the fixed-j_ϕ phases which are described below; at the endpoint the ring has collapsed to the zero temperature Myers-Perry black hole.[10]

---

[10]We had examined the inner and other horizon radii and observed that they remain finite in the limit $\nu \to 1, \lambda \to 2$. This may seem to contradict the collapse of the ring, but one must keep in mind that these radii are defined by the horizon geometry which is discontinuous in the limit.

Curves of constant S^2 angular momentum. The dimensionless angular momentum on the S^2 is given by

$$j_\phi^2 = \frac{\nu(1 + \nu - \lambda)^2(1 + \nu + \lambda)}{2\lambda(1 - \nu)^4} \, . \qquad (4.17)$$

Finding the fixed-j_ϕ curves in the phase diagram can be done by solving $j_\phi = j_\phi^*$ for some fixed value $0 \leq j_\phi^* \leq 1/4$. It is a cubic equation in λ which for $0 < \nu < 1$ and $0 < j_\phi < 1/4$ has three real roots. Two of these roots always violate the constraints (4.1), but the third root satisfies (4.1) provided $\nu > \nu_c(j_\phi^*)$, where $\nu_c(j_\phi^*)$ is some critical value which depends on the value j_ϕ^*.

Figure 6 shows (in light gray) curves of fixed $j_\phi^2 = \frac{1}{500}, \frac{1}{100}, \frac{1}{50}, \frac{1}{35}, \frac{1}{25}, \frac{1}{18}$. For small j_ϕ the curve is very similar to the singly spinning black ring with $j_\phi = 0$, shown in dark gray. The fixed-j_ϕ curves have two endpoints at non-vanishing area $a_{\rm H}$. One corresponds to the limit $\nu \to \nu_c(j_\phi^*)$ which is equivalent to $\lambda \to 2\nu^{1/2}$; this is the zero temperature extremal branch (solid black curve). The other endpoint of the fixed-j_ϕ curves is at $\nu \to 1$, and as shown above the ring collapses to an extremal Myers-Perry black hole in this limit.

When $j_\phi < 1/5$ the fixed j_ϕ-curves have two branches: a thin and a fat ring branch, just like the singly spinning black ring. When $1/5 \leq j_\phi \leq 1/4$ only the thin ring branch exists.

Curve of cusps. The dotted black curve in figure 6 are the position of the cusp of the constant j_ϕ curve, where j_ψ is minimized and the area maximized. The cusp curve is found by using a Lagrange multiplier to fix j_ϕ while extremizing j_ψ. This fixes λ in terms of ν as

$$\lambda = \frac{1}{4}\Big(-1 - \nu + \sqrt{(9 + \nu)(1 + 9\nu)}\Big). \qquad (4.18)$$

The cusp only exists for sufficiently small j_ϕ, namely $j_\phi < 1/5$. The fixed $j_\phi = 1/5$ curve ends at $j_\psi = 4/5$ and $a_{\rm H} = \frac{2}{5}\sqrt{3 + \sqrt{5}}$, where the dotted curve of cusps ends on the dashed curve.

4.3 Physics discussion

One feature of the curves of fixed angular momentum j_ϕ on the S^2 is that the S^1 angular momentum cannot be arbitrarily large. This is easily understood. Recall that in the limit of large j_ψ, the singly rotating black ring becomes large and thin. Non-zero j_ϕ means that the S^2 part of the ring behaves like a Kerr black hole, in particular it will have to obey the Kerr bound on the angular momentum. This implies that for given non-vanishing j_ϕ, the size of the S^2 cannot become arbitrarily thin (the effective S^2 mass cannot be too small because that would violate the Kerr bound). This in turn means that one cannot spin up the ring to arbitrarily large j_ψ. Hence for given j_ϕ, there is a maximum possible value for j_ψ. When j_ϕ is small, the maximum value is large, but decreases as j_ϕ increases, as is seen in figure 6.

Another qualitative feature is the disappearance of the "fat ring branch" as j_ϕ becomes large. Consider two diagonally opposite 2-spheres of the ring. They both carry j_ϕ angular momentum which creates an attractive spin-spin interaction [36]. As the (inner) S^1 decreases, the strength of this spin-spin attraction grows stronger, and it becomes harder to

balance the ring by angular momentum on the S^1. This is what causes the diminishing of the fat ring branch as j_ϕ increases, and for $j_\phi \geq 1/5$, the fat branch disappears.[11]

The analysis of [31] suggested that the thin black ring branch solutions are stable to radial perturbations and the fat rings unstable. This was in concordance with an expected result [37] that at least one extra mode of instability appeared when going across the cusp from the thin black ring branch to the fat black ring branch. Extrapolating these results, doubly spinning rings with large enough S^2 angular momentum, $j_\phi \geq 1/5$, may be expected to be radially stable.

5. Zero-temperature bicycles

We found in section 3 that the symmetric bi-ring system had a zero-temperature limit. In the previous section we investigated a similar zero temperature limit of the doubly spinning black ring, and showed that it corresponded to the collapse of the ring to an extremal Myers-Perry black hole. In this section we take a scaling limit to find a similar collapse zero-temperature limit of the bi-ring solution.

For the symmetric bi-rings the limit of zero temperature is $\kappa_1, \kappa_2 \to \kappa_3 = 1/2$. It is therefore natural to take the limit $\kappa_i \to \kappa$ for some $0 < \kappa < 1$ for the bi-ring solution. This limit corresponds to collapsing all the finite rods in the rod diagram to zero length.

Here we want to take a limit such that $T_1, T_2 \to 0$, but the mass, angular momenta, angular velocities, and horizon areas remain finite. The simplest approach is to first take the limit $\kappa_i \to \kappa$ and then impose the balance conditions, so we also need the r.h.s. of the balance conditions (2.32)–(2.33) to be finite in the limit. Without loss of generality we pick $\kappa = \kappa_1$, and the desired scaling limit is then obtained by setting

$$\kappa_2 = \kappa_1 + w_1 \epsilon\,, \qquad \kappa_3 = \kappa_1 + w_2 \epsilon\,, \qquad \kappa_4 = \kappa_1 + w_3 \epsilon\,, \qquad \kappa_5 = \kappa_1 + \epsilon\,, \tag{5.1}$$

and taking $\epsilon \to 0$. (By exploiting the freedom of rescaling ϵ, we have set the coefficient of ϵ in κ_5 equal to 1.) The ordering of the κ_i implies

$$0 < w_1 < w_2 < w_3 < 1\,. \tag{5.2}$$

The balance conditions become

$$1 \;=\; \frac{w_3(1-w_1)(w_2-w_1)(w_3-w_1)}{w_2^2\,(1-\kappa_1)}\,, \qquad 1 \;=\; \frac{w_3(1-w_1)(w_3-w_1)(w_3-w_2)}{(1-w_2)^2\,\kappa_1}\,. \tag{5.3}$$

One finds that as $\epsilon \to 0$, the temperatures go to zero linearly in ϵ, so the ratio of the temperatures is finite in the limit,

$$\xi = \lim_{\epsilon \to 0}\left(\frac{T_1}{T_2}\right) = \frac{w_2}{(1-w_2)}\sqrt{\frac{(1-w_1)(1-w_3)}{w_1\,w_3}}\,. \tag{5.4}$$

This ratio can take any non-negative value, and the limit $T_1, T_2 \to 0$ can therefore be taken along any subfamily of solutions with $T_1 = \xi\,T_2$ for any value of ξ.

---

[11]We are grateful to R. Emparan for discussions of these properties.

In the scaling limit we find (superscript "(0)" indicates zero temperature)

$$M^{(0)} \;=\; \frac{3\pi\,L^2}{4G}\,, \qquad J_\phi^{(0)} \;=\; \frac{\pi\,L^3}{\sqrt{2}\,G}\,(1-\kappa_1)\,, \qquad J_\psi^{(0)} \;=\; \frac{\pi\,L^3}{\sqrt{2}\,G}\,\kappa_1\,. \qquad (5.5)$$

Note that the relationship between the mass-fixed angular momenta are exactly the same as for the extremal Myers-Perry black hole. We therefore expect the limit to be a collapse of the two orthogonal rings to a single extremal Myers-Perry black hole, just as in the $\nu \to 1, \lambda \to 2$ limit of the doubly spinning black ring. Again, the horizon areas will be discontinuous in this limit, so the corresponding limiting curves in the phase diagram do not correspond to physical black hole phases.

Even if the zero temperature limit of the bi-ring solution presented in this paper turns out to simply give the extremal Myers-Perry black hole, we do expect there to exist zero temperature bi-ring system. These are obtained from a more general bi-ring system, constructed from two rings which each carry intrinsic angular momenta on both S^1 and S^2. For this more general bi-ring the limit of extremality is similar to the $\lambda \to 2\sqrt{\nu}$ limit of each of the doubly spinning black rings of the system. We expect those extremal solutions to have arbitrarily large angular momenta in both planes. In the next section we discuss the zero temperature phase diagram.

6. Discussion

In this paper we have analyzed two 4+1-dimensional asymptotically flat black hole vacuum solutions: one is the doubly spinning black ring, the other is the bicycling black rings, the bi-rings, consisting of two black rings balanced in orthogonal planes. Both solutions are constructed by the inverse scattering method. The doubly spinning black ring was found by Pomeransky and Sen'kov [18], and the bi-ring solution constructed here is new.

We showed in section 4 that the doubly spinning black ring had two limits of zero temperature. The first of these limits, $\lambda \to 2\sqrt{\nu}$, gives a zero-temperature extremal doubly rotating black ring. We have proven that good coordinates exist across the horizon, so indeed the solution is regular everywhere on and outside the horizon. This branch of zero temperature vacuum solution shares certain features with supersymmetric black rings, for instance that the inner and outer horizon radii are the same. However, there are also clear differences, for example that the extremal non-supersymmetric rings have non-vanishing angular velocities, while $\Omega = 0$ for asymptotically flat supersymmetric black holes. This difference is significant for studying dragging in the system. Remarkably, Reall has shown [38] that the entropy of this non-supersymmetric extremal black ring can be reproduced from a microscopic calculation.

In the other extremal limit ($\nu \to 1, \lambda \to 2$) of the doubly spinning ring, we have shown that the ring collapses to a zero-temperature Myers-Perry black hole.

Figure 7 shows the known phases of zero temperature single horizon vacuum black holes: the zero temperature Myers-Perry black hole and the extremal limit of the doubly spinning black ring. The two phase diagrams, (a) and (b), shown in figure 7 are equivalent. In figure (a) we use the S^1 angular momentum j_ψ of the ring as the "order parameter"
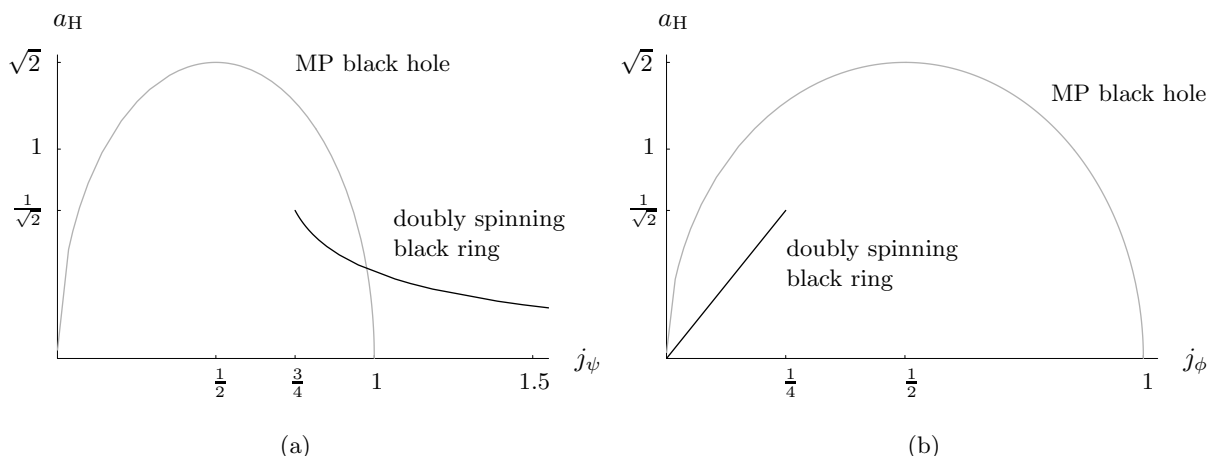
Figure 7: Phase diagram for zero temperature single horizon black holes. In figure (a) we choose the S^1 angular momentum of the doubly spinning ring on the horizontal axis, in figure (b) it is the S^2 angular momentum. The *gray* curve is the zero temperature Myers-Perry black hole. Its entropy is maximized when the system is symmetric, i.e. when $j_\psi = j_\phi = 1/2$. The *solid* black curve is the regular zero temperature limit $\lambda \to 2\nu^{1/2}$ of the doubly spinning black ring. It reaches maximum area $a_{\rm H} = 1/\sqrt{2}$ for maximal $j_\phi = 1/4$ and minimal $j_\psi = 3/4$.

on the horizontal axis, and in figure (b) it is the S^2 angular momentum. There is no non-uniqueness in the phase diagram in figure 7, because the two solutions never co-exist with the same j_ψ and j_ϕ.

In addition to the single horizon phases shown in figure 7 there will exist other zero temperature phases for 4+1-dimensional vacuum black holes. These include extremal bi-rings and extremal saturn solutions. The bi-rings we have constructed in this paper are a subclass of a more general family of bi-ring solutions. Recall that our bi-rings are essentially superpositions of singly spinning black rings. Obviously one can construct more general solutions by superimposing the doubly spinning black rings. This would presumably require using a two-step solution generating procedure with the second step involving a non-diagonal seed, as in [18].

When the S^2's of the generalized bi-ring system carry maximal spin, one expects to have a zero temperature bi-ring configuration consisting of two doubly spinning extremal black rings. The general bi-ring system is expected to have a 3-fold continuous non-uniqueness corresponding to the freedom of distributing the mass and the two angular momenta between the two black objects while keeping the total asymptotic ADM mass and angular momenta fixed and imposing balance. Requiring zero temperature for each ring gives two constraints, and the degeneracy reduces to 1-fold continuous non-uniqueness for the extremal bi-rings. Thus these solutions will fill up a 2d area of the phase diagram.

And even more non-uniqueness can be expected. Figure 8 shows our expectations for the full phase diagram of *extremal* doubly rotating 4+1-dimensional asymptotically flat vacuum black holes. The curves are the single horizon solutions shown also in figure 7(a). The gray strip covers the phase diagram from $j = 0$ to arbitrarily large j. The total area is bounded by the maximum of the zero temperature Myers-Perry black hole, so that the gray strip covers $j \geq 0$ and $0 < a_{\rm H}^{\rm total} < \sqrt{2}$. The proposal is that there exist zero temperature
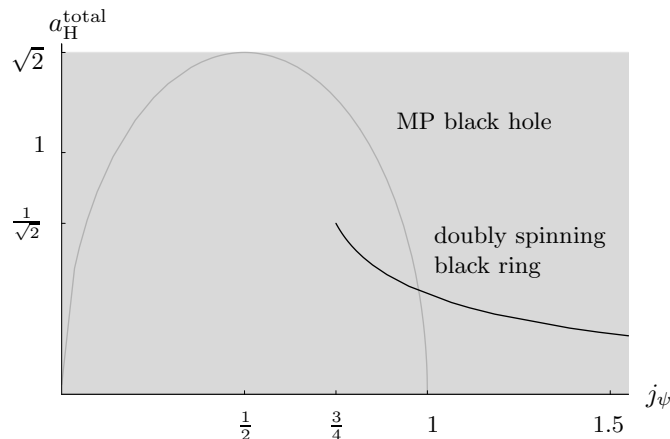
Figure 8: Expected phase diagram for zero temperature extremal 4+1-dimensional asymptotically flat vacuum black holes. Extremal bi-ring saturn configurations are anticipated to fully cover the gray strip with $0 \leq j < \infty$ and $0 < a_{\text{total}} < \sqrt{2}$. In addition, generalized extremal bi-ring solutions will provide further non-uniqueness in the system.

black hole solutions at any point of the gray strip.

The analysis behind this is similar to the one done for the phase diagram of the non-extremal singly spinning black holes in [10]. One way to justify that the whole strip in the phase diagram is covered by solutions is to consider the system of a zero temperature Myers-Perry black hole surrounded by a zero temperature doubly spinning black ring; this is the natural zero temperature black saturn solution. One can get arbitrarily close to the upper bound $a_{\text{H}}^{\text{total}} = \sqrt{2}$ by putting most of the mass in the Myers-Perry black hole, and tuning its angular momentum to maximize its entropy. The *total* angular momentum in one plane of rotation can then be adjusted to be any value $0 \leq j < \infty$ by including a thin zero temperature black ring around the black hole. The angular momentum in the orthogonal plane can likewise be adjusted to any value by including a second black ring, thus combining the bi-rings and black saturn into a black bi-ring saturn.[12]

We expect that any balanced zero temperature black hole configuration in 4+1-dimensional vacuum gravity, with asymptotically flat boundary conditions, have total dimensionless area bounded by $a_{\text{H}}^{\text{total}} = \sqrt{2}$, which is the maximal area of the zero temperature Myers-Perry black hole. It is achieved for $j_\psi = j_\phi$. For comparison, it was argued in [10] that non-extremal black hole configurations exist of any j and any total area $a_{\text{H}}^{\text{total}} \leq 2\sqrt{2}$. The inequality is saturated only for the static 4+1-dimensional Schwarzschild solution.

The continuous non-uniqueness in the general non-extremal black hole phase diagram can be arbitrarily large. A system consisting of n concentric doubly spinning black rings distributed at will in the two orthogonal planes and surrounding a central doubly spinning black hole will have $3n$-fold continuous non-uniqueness. There are only 3 conserved quantities, the ADM mass and two angular momenta, but these can be distributed continuously (at least classically) between the $n + 1$ objects (subject to balance conditions). In addition to this, there can be discrete non-uniqueness. Imposing thermodynamic equilibrium, equal

---

[12]Having arbitrarily large angular momentum relies on the space being infinite since the ring needs to be large. So if the system is put in a box, the phase structure would necessarily change.

temperatures and equal angular velocities, is expected to fix the radius of the rings, so the most general equilibrium system would be the bi-ring saturn discussed above.

Higher dimensional gravity has proven to contain an intriguing richness of black hole solutions. We are privileged to be able to access some of them as exact solutions. Although these are in some cases rather involved solutions, like black saturn and the bi-rings, it is possible to extract interesting physics. In general, we cannot expect to be lucky to have exact solutions for all interesting black hole configurations, and other methods for constructing solutions are needed. Recently the matched asymptotic expansion method was used to construct large radius higher dimensional black rings [39]. From these solutions interesting properties of the phase diagram of black holes were extracted and the remaining structure of the phase diagram conjectured. Just like black saturn had a place in that phase diagram, so will doubly spinning black rings, bi-rings and bi-ring saturns in the generalization to involve spin in both planes of rotation.

In this paper we have examined extremal limits of exact black hole solutions. A common picture seems to be that if a rod diagram description of the solution can be given, then the zero temperature extremal limit is a scaling limit in which the finite length rods shrink to zero size. This characterization may lead to simplifications for constructing extremal black hole configurations; it would be interesting and useful if it could be implemented directly in the inverse scattering method.

Acknowledgments

A. Horizon metrics

The BZ parameters introduced by the soliton transformations are dimensionful. It is more natural to rescale them $b_2 L^{-1} \to b_2$ and $c_1 L^{-1} \to c_1$ to make them dimensionless. The

rescaled parameters are used in this appendix. It is implicitly understood that c_1 and b_2 are fixed by (2.27).

The bi-ring solution has two disconnected horizons, each with topology $S^1 \times S^2$. Here we give the metric on the event horizons. The ring with event horizon located at $\rho = 0$ and $\kappa_1 \leq \bar{z} \leq \kappa_2$ is refered to as ring 1, and the one with event horizon at $\rho = 0$ and $\kappa_4 \leq \bar{z} \leq \kappa_5$ is ring 2.

Black ring 1. The metric on the horizon of ring 1 is

$$
ds^2_{\text{BR1}} = \frac{L^2 \, s^2_{\text{BR1}} \, f_1(\bar{z})}{(\bar{z} - \kappa_1)(\kappa_2 - \bar{z})} \, d\bar{z}^2
$$
$$
+ \frac{L^2 \, \bar{z} \, (\bar{z} - \kappa_1)(\kappa_2 - \bar{z})^2}{(1 - \bar{z})(\kappa_4 - \bar{z}) \, f_1(\bar{z})} \left[b_2^{-1} d\psi + c_1^{-1} \frac{\kappa_1 (1 - \bar{z})}{\bar{z}} \, d\phi \right]^2
$$
$$
+ \frac{L^2 \, (\bar{z} - \kappa_1)^2 (\kappa_2 - \bar{z})(\kappa_4 - \bar{z})}{2 \, \bar{z}(\kappa_3 - \bar{z})(\kappa_5 - \bar{z}) \, f_1(\bar{z})} \, d\phi^2 + \frac{L^2 \, (\kappa_3 - \bar{z})(\kappa_5 - \bar{z})}{2 \, (1 - \bar{z}) \, f_1(\bar{z})} \, d\psi^2, \quad \text{(A.1)}
$$

where $\bar{z} \in [\kappa_1, \kappa_2]$ and

$$
s_{\text{BR1}} = \frac{\sqrt{2 \, \kappa_2 \, \kappa_3 \, \kappa_5 \, (1 - \kappa_1)(\kappa_2 - \kappa_1)(\kappa_4 - \kappa_1)}}{\kappa_4 \, (\kappa_3 - \kappa_1)(\kappa_5 - \kappa_1)}, \quad \text{(A.2)}
$$
$$
f_1(\bar{z}) = \frac{(\bar{z} - \kappa_1)(\kappa_4 - \bar{z})}{4 \, \bar{z} \, (1 - \bar{z})} + c_1^{-2} \frac{\kappa_1^2 \, (\kappa_2 - \bar{z})(\kappa_3 - \bar{z})(\kappa_5 - \bar{z})}{2 \, \bar{z} \, (\kappa_4 - \bar{z})} + b_2^{-2} \frac{(\bar{z} - \kappa_1)^2 (\kappa_2 - \bar{z})^2}{2 (1 - \bar{z})(\kappa_3 - \bar{z})(\kappa_5 - \bar{z})}.
$$

The horizon area is $A_1 = (2\pi)^2 \, L^3 \, (\kappa_2 - \kappa_1) \, s_{\text{BR1}}$.

Black ring 2. The metric on the horizon of ring 2 is

$$
ds^2_{\text{BR2}} = \frac{L^2 \, s^2_{\text{BR2}} \, f_2(\bar{z})}{(\bar{z} - \kappa_4)(\kappa_5 - \bar{z})} \, d\bar{z}^2
$$
$$
+ \frac{L^2 \, (1 - \bar{z})(\bar{z} - \kappa_4)^2 (\kappa_5 - \bar{z})}{4 \, \bar{z} \, (\bar{z} - \kappa_2) \, f_2(\bar{z})} \left[c_1 \, \kappa_5^{-1} \, d\phi + b_2 \frac{(1 - \kappa_5)}{(1 - \kappa_1)} \frac{\bar{z}}{(1 - \bar{z})} \, d\psi \right]^2
$$
$$
+ \frac{L^2 \, (\bar{z} - \kappa_1)(\bar{z} - \kappa_3)}{2 \, \bar{z} \, f_2(\bar{z})} \, d\phi^2 + \frac{L^2 \, (\bar{z} - \kappa_2)(\bar{z} - \kappa_4)(\kappa_5 - \bar{z})^2}{2(\bar{z} - \kappa_1)(\bar{z} - \kappa_3)(1 - \bar{z}) \, f_2(\bar{z})} \, d\psi^2, \quad \text{(A.3)}
$$

where $\bar{z} \in [\kappa_4, \kappa_5]$ and

$$
s_{\text{BR2}} = \frac{\sqrt{2 \, \kappa_5 \, (1 - \kappa_1)(1 - \kappa_3)(1 - \kappa_4)(\kappa_5 - \kappa_4)(\kappa_5 - \kappa_2)}}{(1 - \kappa_2)(\kappa_5 - \kappa_1)(\kappa_5 - \kappa_3)}, \quad \text{(A.4)}
$$
$$
f_2(\bar{z}) = \frac{(\bar{z} - \kappa_2)(\kappa_5 - \bar{z})}{4 \, \bar{z} \, (1 - \bar{z})} + c_1^2 \frac{(\bar{z} - \kappa_4)^2 (\kappa_5 - \bar{z})^2}{8 \, \kappa_5^2 \, \bar{z} \, (\bar{z} - \kappa_1)(\bar{z} - \kappa_3)}
$$
$$
+ b_2^2 \frac{(1 - \kappa_5)^2 (\bar{z} - \kappa_1)(\bar{z} - \kappa_3)(\bar{z} - \kappa_4)}{8(1 - \kappa_1)^2 (1 - \bar{z})(\bar{z} - \kappa_2)}.
$$

The horizon area is $A_2 = (2\pi)^2 \, L^3 \, (\kappa_5 - \kappa_4) \, s_{\text{BR2}}$.

Note that the functions f_1 and f_2 are manifestly positive.
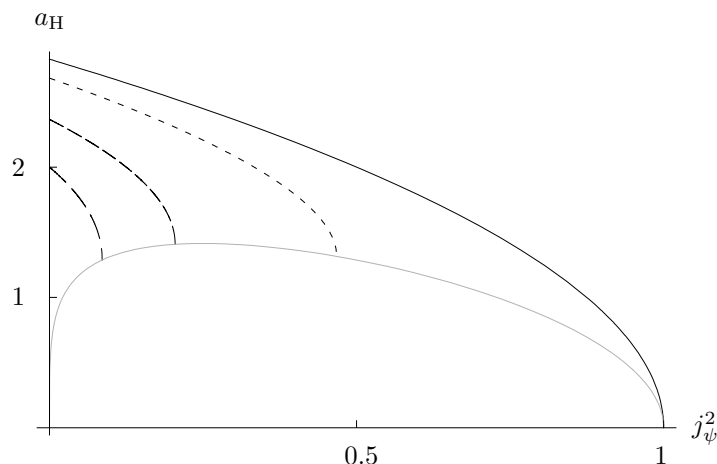
Figure 9: Phase diagram for the Myers-Perry black hole in five dimensions. The *dashed* lines show to Myers-Perry black hole phases for fixed values of $j_\phi^2 = 1/10,\ 3/10,\ 5/10$ (right to left). The five dimensional singly spinning black hole, *solid* curve, becomes singular in the limit $j_\psi \to 1$ The *gray* curve is the phase of the zero temperature extremal Myers-Perry black holes.

B. Myers-Perry black hole

In 4+1 dimensions, the ADM mass and the two angular momenta in orthogonal planes of the Myers-Perry black hole [23] are

$$M = \frac{3\,\pi\,\mu}{8\,G}\,, \qquad J_\phi = \frac{\pi\,\mu\,a_1}{4\,G}\,, \qquad J_\psi = \frac{\pi\,\mu\,a_2}{4\,G}\,. \tag{B.1}$$

and the horizon area is

$$A_{\mathrm{H}} = \sqrt{2}\,\pi^2\,\mu \left[\mu - a_1^2 - a_2^2 + \left[(\mu - a_1^2 - a_2^2)^2 - 4\,a_1^2 a_2^2 \right]^{1/2} \right]^{1/2} \tag{B.2}$$

Here μ, a_1 and a_2 are the mass and rotation parameters respectively. They must satisfy the condition

$$\mu \geq a_1^2 + a_2^2 + 2\,|a_1\,a_2| \tag{B.3}$$

to ensure the existence of an event horizon.

The single spinning Myers-Perry black hole shrinks to zero size while reaching its maximum angular momentum at $j = 1$, where the solution becomes singular. This behaviour changes as the angular momentum in the orthogonal plane is turned on. An extremal non-zero minimum of the horizon area is then reached at maximum momentum. This is shown in figure 9. The endpoints of the fixed-j_ϕ curves all have zero temperature. The phase of extremal Myers-Perry black holes is shown as the gray curve in figure 9. It is obtained by saturating the bound (B.3), which implies that the inner and outer horizons coincide, so that the solution is extremal and has zero temperature.

References

[1] A. Strominger and C. Vafa, *Microscopic origin of the Bekenstein-Hawking entropy*, *Phys. Lett.* **B 379** (1996) 99 [hep-th/9601029].

[2] H. Elvang and R. Emparan, *Black rings, supertubes and a stringy resolution of black hole non-uniqueness*, *JHEP* **11** (2003) 035 [`hep-th/0310008`].

[3] R. Emparan, *Rotating circular strings and infinite non-uniqueness of black rings*, *JHEP* **03** (2004) 064 [`hep-th/0402149`].

[4] H. Elvang, R. Emparan and P. Figueras, *Non-supersymmetric black rings as thermally excited supertubes*, *JHEP* **02** (2005) 031 [`hep-th/0412130`].

[5] F. Larsen, *Entropy of thermally excited black rings*, *JHEP* **10** (2005) 100 [`hep-th/0505152`].

[6] R. Emparan and G.T. Horowitz, *Microstates of a neutral black hole in M-theory*, *Phys. Rev. Lett.* **97** (2006) 141601 [`hep-th/0607023`].

[7] G.T. Horowitz and M.M. Roberts, *Counting the microstates of a Kerr black hole*, *Phys. Rev. Lett.* **99** (2007) 221601 [`arXiv:0708.1346`].

[8] O.J.C. Dias, R. Emparan and A. Maccarrone, *Microscopic theory of black hole superradiance*, *Phys. Rev.* **D 77** (2008) 064018 [`arXiv:0712.0791`].

[9] H. Elvang and P. Figueras, *Black saturn*, *JHEP* **05** (2007) 050 [`hep-th/0701035`].

[10] H. Elvang, R. Emparan and P. Figueras, *Phases of five-dimensional black holes*, *JHEP* **05** (2007) 056 [`hep-th/0702111`].

[11] R. Emparan and H.S. Reall, *A rotating black ring in five dimensions*, *Phys. Rev. Lett.* **88** (2002) 101101 [`hep-th/0110260`].

[12] H. Iguchi and T. Mishima, *Black di-ring and infinite nonuniqueness*, *Phys. Rev.* **D 75** (2007) 064018 [`hep-th/0701043`].

[13] J. Evslin and C. Krishnan, *The black di-ring: an inverse scattering construction*, `arXiv:0706.1231`.

[14] T. Mishima and H. Iguchi, *New axisymmetric stationary solutions of five-dimensional vacuum Einstein equations with asymptotic flatness*, *Phys. Rev.* **D 73** (2006) 044030 [`hep-th/0504018`].

[15] S. Tomizawa, Y. Morisawa and Y. Yasui, *Vacuum solutions of five dimensional Einstein equations generated by inverse scattering method*, *Phys. Rev.* **D 73** (2006) 064009 [`hep-th/0512252`].

[16] P. Figueras, *A black ring with a rotating 2-sphere*, *JHEP* **07** (2005) 039 [`hep-th/0505244`].

[17] H. Kudoh, *Doubly spinning black rings*, *Phys. Rev.* **D 75** (2007) 064006 [`gr-qc/0611136`].

[18] A.A. Pomeransky and R.A. Sen'kov, *Black ring with two angular momenta*, `hep-th/0612005`.

[19] R. Emparan and H.S. Reall, *Black rings*, *Class. and Quant. Grav.* **23** (2006) R169 [`hep-th/0608012`].

[20] Y. Morisawa, S. Tomizawa and Y. Yasui, *Boundary value problem for black rings*, *Phys. Rev.* **D 77** (2008) 064019 [`arXiv:0710.4600`].

[21] J.P. Gauntlett and J.B. Gutowski, *Concentric black rings*, *Phys. Rev.* **D 71** (2005) 025013 [`hep-th/0408010`]; *General concentric black rings*, *Phys. Rev.* **D 71** (2005) 045002 [`hep-th/0408122`].

[22] I. Bena, C.-W. Wang and N.P. Warner, *Sliding rings and spinning holes*, *JHEP* **05** (2006) 075 [`hep-th/0512157`].

[23] R.C. Myers and M.J. Perry, *Black holes in higher dimensional space-times*, *Ann. Phys. (NY)* **172** (1986) 304.

[24] K. Izumi, *Orthogonal black di-ring solution*, `arXiv:0712.0902`.

[25] A.A. Pomeransky, *Complete integrability of higher-dimensional Einstein equations with additional symmetry and rotating black holes*, *Phys. Rev.* **D 73** (2006) 044004 [`hep-th/0507250`].

[26] V.A. Belinsky and V.E. Zakharov, *Integration of the Einstein equations by the inverse scattering problem technique and the calculation of the exact soliton solutions*, *Sov. Phys. JETP* **48** (1978) 985 [*Zh. Eksp. Teor. Fiz.* **75** (1971) 1953].

[27] V.A. Belinsky and V.E. Sakharov, *Stationary gravitational solitons with axial symmetry*, *Sov. Phys. JETP* **50** (1979) 1 [*Zh. Eksp. Teor. Fiz.* **77** (1979) 3].

[28] V. Belinski and E. Verdaguer, *Gravitational solitons*, Cambridge University Press, Cambridge U.K. (2001).

[29] R. Emparan and H.S. Reall, *Generalized Weyl solutions*, *Phys. Rev.* **D 65** (2002) 084025 [`hep-th/0110258`].

[30] T. Harmark, *Stationary and axisymmetric solutions of higher-dimensional general relativity*, *Phys. Rev.* **D 70** (2004) 124002 [`hep-th/0408141`].

[31] H. Elvang, R. Emparan and A. Virmani, *Dynamics and stability of black rings*, *JHEP* **12** (2006) 074 [`hep-th/0608076`].

[32] H.K. Kunduri, J. Lucietti and H.S. Reall, *Near-horizon symmetries of extremal black holes*, *Class. and Quant. Grav.* **24** (2007) 4169 [`arXiv:0705.4214`].

[33] H. Elvang, R. Emparan, D. Mateos and H.S. Reall, *A supersymmetric black ring*, *Phys. Rev. Lett.* **93** (2004) 211302 [`hep-th/0407065`].

[34] H. Elvang, R. Emparan, D. Mateos and H.S. Reall, *Supersymmetric black rings and three-charge supertubes*, *Phys. Rev.* **D 71** (2005) 024033 [`hep-th/0408120`].

[35] I. Bena and N.P. Warner, *One ring to rule them all ... and in the darkness bind them?*, *Adv. Theor. Math. Phys.* **9** (2005) 667 [`hep-th/0408106`].

[36] R. Wald, *Gravitational spin interaction*, *Phys. Rev.* **D 6** (1972) 406.

[37] G. Arcioni and E. Lozano-Tellechea, *Stability and critical phenomena of black holes and black rings*, *Phys. Rev.* **D 72** (2005) 104021 [`hep-th/0412118`]; *Stability and thermodynamics of black rings*, `hep-th/0502121`.

[38] H.S. Reall, *Counting the microstates of a vacuum black ring*, `arXiv:0712.3226`.

[39] R. Emparan, T. Harmark, V. Niarchos, N.A. Obers and M.J. Rodriguez, *The phase structure of higher-dimensional black rings and black holes*, *JHEP* **10** (2007) 110 [`arXiv:0708.2181`].